Science of the Total Environment 768 (2021) 144997

Contents lists available at ScienceDirect

Science of the Total Environment

journal homepage: www.elsevier.com/locate/scitotenv

Delineation of hydrocarbon contaminants with multi-frequency complex conductivity imaging

Adrián Flores Orozco [a,*], Paolo Ciampi [e], Timea Katona [a], Matteo Censini [d], Marco Petrangeli Papini [b], Gian Piero Deidda [c], Giorgio Cassiani [d]

[a] Dept. of Geodesy and Geoinformation, TU Wien, Vienna, Austria
[b] Dept. of Chemistry, University of Rome "La Sapienza", Rome, Italy
[c] Dept. of Civil and Environmental Engineering and Architecture, University of Cagliari, Cagliari, Italy
[d] Dept. of Geosciences, University of Padova, Padova, Italy
[e] Department of Earth Sciences, University of Rome "La Sapienza", Rome, Italy

HIGHLIGHTS

- Interpretation of 1D laser-induced fluorescence logs and complex electrical imaging
- Imaging trapped fuel in the subsurface through 2D complex conductivity and 1D LIF
- Geophysical electrical imaging and borehole methods to investigate a jet fuel spill
- Interpretation of electrical anomalies related to geology and LNAPLs
- IP increases in dissolved plume and negligible in free-phase LNAPLs.

GRAPHICAL ABSTRACT

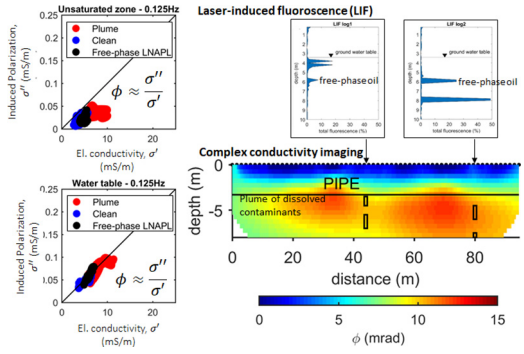

ARTICLE INFO

Article history:
Received 25 September 2020
Received in revised form 15 December 2020
Accepted 15 December 2020
Available online 8 January 2021

Editor: Thomas Kevin V

Keywords:
Jet fuel
Hydrocarbon contamination
Noninvasive methods
Near surface geophysics

ABSTRACT

The characterization of contaminated sites is a serious issue that requires a number of techniques to be deployed in the field to reconstruct the geometry, hydraulic properties and state of contamination of the shallow subsurface, often at the hundreds of meter scale with metric resolution. Among the techniques that have been proposed to complement direct investigations (composed of drilling, sampling, and laboratory characterization) are geophysical methods, which can provide extensive spatial coverage both laterally and at depth with the required resolution. However, geophysical methods only measure physical properties that are indirectly related to contamination, and their correlation may be difficult to ascertain without direct ground truth. In this study, we present a successful example where the results of complex conductivity measurements conducted in an imaging framework are compared with direct evidence of subsoil contamination at a jet fuel impacted site. Thus, proving that a combination of direct and indirect investigations can be successfully used to image a site in its complex (potentially 3D) structure in order to build a reliable conceptual model of the site.

1. Introduction

Organic compounds, such as chlorinated hydrocarbons (CHCs), polycyclic aromatic hydrocarbons (PAHs), aromatic hydrocarbons (e.g., the BTEX group: benzene, toluene, ethyl benzene and xylene), phenols etc. represent the main contaminants affecting soil and

* Corresponding author.
E-mail address: adrian.flores-orozco@geo.tuwien.ac.at (A. Flores Orozco).

https://doi.org/10.1016/j.scitotenv.2021.144997

groundwater in Europe (Panagos et al., 2013). Kerosene is a petroleum hydrocarbon, widely used as fuel, which represents a common and persistent soil contaminant as a result of leakages from storage tanks and transport pipes, as well as accidental spills. Similar to other petroleum fuels, kerosene is a light non-aqueous phase liquid (LNAPL), as it is only marginally soluble in water and it is less dense (i.e., lighter) than it. Therefore, kerosene spills infiltrate into the soil and initially rest upon the water table. Yet, as time progresses, LNAPLs can reach deeper zones following fluctuations of groundwater level. Due to the lack of ionic or polar groups, "non-polar" compounds, such as kerosene, form non-miscible discrete droplets within the water-filled pores and without a direct contact with the grain surface. NAPLs thus generally are the non-wetting phase, unless strong fractions of organic matter are present as solid phase in the soil.

Over time, hydrocarbon-contaminant plumes face biotic and abiotic chemical transformations leading to the depletion of soluble and volatile compounds (Totsche et al., 2003) as well as changes in the ionic composition, turning hydrocarbon fuels into polar compounds (Haagh et al., 2020). In particular, petroleum hydrocarbons such as kerosene are easily prone to biotic degradation under both aerobic and anaerobic conditions, which results in changes in the wettability and mobility of the contaminant (e.g., Bennett et al., 2004). Accordingly, understanding the distribution and chemical transformations of fuel hydrocarbon-plumes is a critical first step towards an adequate management and remediation of contaminated sites (Tang et al., 2012; Lari et al., 2018).

To date, site characterization still relies for the most part on direct methods, i.e. methods based on direct measurements of contaminant concentrations in air, soil and water samples. However, it has been demonstrated that direct methods are limited in the spatial and temporal resolution of the information (e.g., Cassiani et al., 2014; Binley et al., 2015; Flores Orozco et al., 2019a), and might result in a poor estimation on the concentration and extension of hydrocarbon-plumes (Algreen et al., 2015; McCall et al., 2018). Moreover, the investigation of extensive areas with high spatial and temporal resolution by means of direct methods is prohibitively expensive. To overcome such serious limitations, geophysical electrical methods, such as electrical resistivity tomography (ERT), have been widely applied for the characterization and monitoring of contaminant plumes (e.g., Sauck, 2000; Chambers et al., 2010; Heenan et al., 2015; Naudet et al., 2014). These attempts partly relied on the high electrical resistivity of free-phase hydrocarbons, and largely on the observation that chemical transformations of the hydrocarbon plumes result in a significant decrease in the electrical resistivity due to the weathering of grains, increase in the fluid conductivity, accumulation of microbial cells and metabolic products such as carbonic acids (e.g., Cassidy et al., 2001; Werkema Jr et al., 2003; Atekwana et al., 2004). Hence, fresh spills often show high electrical resistivity values (albeit such "freshness" is quick to disappear), while aged hydrocarbon contaminant plumes commonly result in electrical conductive anomalies (for a review we refer to the studies by Che-Alota et al., 2009; Atekwana and Atekwana, 2010; Caterina et al., 2017; Heenan et al., 2013).

Although ERT offers the potential to delineate the spatial extent of hydrocarbon contaminant plumes as well as possible transformation of the pollutant, variations in the geological features of the subsurface might challenge the interpretation of electrical signatures. For instance, conductive anomalies can be observed for areas with high clay content and bear no relevance to the processes of biodegradation in aged hydrocarbon contaminants; while high resistivity values can indicate a decrease in saturation, the contact to compacted rocks or the fresh spills.

In search for an alternative non-invasive hydrocarbon detection method, over the last decade several studies have evaluated the applicability of the complex resistivity (CR) or complex conductivity (CC) method for the characterization of contaminant plumes. Also known as the induced polarization (IP) method, this is an extension of ERT, which provides information in terms of the real (σ') and imaginary (σ'') components of the complex conductivity (σ^*). Briefly, the method is based on four electrode arrays, where a pair of electrodes are used to inject a current to the ground and the other pair is used to measure the resulting electrical impedance. The electrical field imposed into the ground by galvanic current injection forces the migration of free ions in the electrolyte (associated to the electrical conductivity measured in ERT or in the real component, σ'), while part of the ions accumulate at the electrical double layer (EDL) formed at the interface between the grains and the fluid. The imposed electrical field also forces a polarization of the ions accumulated at the EDL, with σ'' expressing the strength of such induced polarization, which is a measure of the capacitive (i.e., electrostatic energy storage) properties of the subsurface. Initial studies (Vanhala, 1997; Olhoeft, 1985; Kemna et al., 2004; Schmutz et al., 2010) revealed an increase in the IP effect with increasing concentrations of non-polar hydrocarbons in soils, such as toluene, benzene, which are compounds typically found in kerosene. However, recent studies (Cassiani et al., 2009; Ustra et al., 2012; Schwartz et al., 2012; Shefer et al., 2013) reported a negligible polarization response in laboratory measurement for similar compounds. At the field scale, the studies by Kemna et al. (2004) and Deceuster and Kaufmann (2012) reported an increase in the electrical conductivity and polarization response with increasing the concentrations of kerosene and benzene (respectively); while the studies by Blondel et al. (2014) and Maurya et al. (2018) report no effect in the IP response in a site impacted by benzene, yet a reduction in the electrical conductivity. Flores Orozco et al. (2012a) revealed a linear increase in the IP response with increasing benzene concentration in groundwater samples, but only below saturation concentration; while higher concentrations as well as the presence of the LNAPL in free-phase, exhibited an abrupt decrease in the IP response to values close to zero. Bücker et al. (2017) explains such a change as a consequence of the changes imposed in the pore-space geometry. Based on such model, immiscible oil droplets trapped within the large pores result in the formation of smaller pores for the displaced pore-water with an increase in the pore-space tortuosity, which hinder the free movement of the ions in the pore-water and, thus, enhance the polarization response. Accordingly, at higher concentrations, hydrocarbons are trapped within both big and small pores forming a continuous phase, while the pore-water is found as a continuous film surrounding the grains where the ions can migrate; thus, hindering polarization effects. Alternatively, disconnections in Stern layer (the interior part of the EDL) have been suggested as the mechanism explaining the observed increase in the polarization response with increasing the volumetric content of non-polar compounds (e.g., Schmutz et al., 2010). However, such mechanism cannot explain the lack of a measurable polarization observed in the lab (e.g., Cassiani et al., 2009; Ustra et al., 2012) or, for high LNPAL concentrations at the field-scale (Cassiani et al., 2014; Flores Orozco et al., 2012a, 2019a, 2019b). Moreover, it has been observed that the production of bio-surfactants in mature plumes can result in modifications in the surface electrical properties of the hydrocarbons (e.g., Cassidy et al., 2001) and, for instance, promote a change from "non-wetting" oil to "wetting" oil. Bio-surfactants are produced by bacteria in order to help emulsify the oil and make it thus more bio-available. Previous studies in the laboratory (e.g., Revil et al., 2011) have observed a decrease in the polarization response for sediments impacted by wetting-oils, explaining it by the modification of the electrical properties of the grain surface, and thus, the EDL. Additionally, the changes in the IP response of contaminated sites have been explained as being caused by the accumulation of microbial cells or biofilm formation, as also observed in lab measurements (e.g., Abdel Aal et al., 2006; Atekwana and Slater, 2009), or by the accumulation of iron sulphides due to the stimulation of iron-reducing bacteria (Mewafy et al., 2013; Abdel Aal and Atekwana, 2014). The potential of the CC method to both textural and chemical properties of the pore-space has also prompted its application to characterize changes in the hydraulic conductivity (e.g., Revil and Florsch, 2010), which has been recently applied by Maurya et al. (2018) to solve for hydraulic parameters in hydrocarbon-contaminated sites.

It is clear that the CC method has a great potential to delineate spatial variations in hydrocarbon-contaminant plumes as well as possible biogeochemical transformations in the pollutants, and both types of information is needed for the design of field remediation strategies (Flores Orozco et al., 2015, 2019a). However, the lack of a universal model predicting the electrical response in presence of jet fuel contaminants, in particular at the field scale, demands further investigations. To this end, in this study we investigate variations in the CC response for data collected in the vicinity of the military airport of Decimomannu (Cagliari, Italy), where aviation fuel spills have been reported in 2007 (~40 m^3), in 2009 (~5 m^3), and in 2010 (~5 m^3).

We conducted CC imaging (hereafter CCI) surveys in the area placed hydrogeologically down gradient of the military base, at the edge of the well-known kerosene contaminant plume. Measurements were collected along different profiles with the objective to evaluate changes in the electrical signatures related to the presence of contaminant in free-phase and at lower concentrations in the plume of dissolved contaminants, as well as in areas where we expect clean sediments. Borehole information at the study area permits the interpretation and evaluation of the CCI results. In particular, the thickness of LNAPL in free-phase is known at particular positions through laser induced fluorescence (LIF) loggings, and measurements in soil samples. Due to the available information, the site offers an excellent opportunity to investigate changes in the electrical response for variations in the concentration of jet fuels. Moreover, interpretation of the CCI results should permit to evaluate the extension of the jet fuel contaminant plume down-gradient from the military station and evaluate current models based on the extrapolation of borehole data. Hence, a second objective in our study is to addresses the combination of innovative direct and indirect methods, such the LIF logging and quasi-continuous CCI, with the combination of these techniques also being investigated for first time.

2. Material and methods

2.1. Geological and hydrogeological description of the site: the conceptual model

We conducted complex conductivity imaging (CCI) measurements in May 2019 to investigate the extent of the kerosene contaminant plume down-gradient (as illustrated in Fig. 1) of the military base located at Decimomannu (Italy). The study area corresponds to a depositional sequence of Plio-Quaternary alluvial sediments, where materials recovered from the drilling of seven boreholes (BH1 to BH7) permitted to develop the geological cross-section presented in Fig. 1a. Such geological cross-section represents the conceptual model in our study, characterized by five roughly horizontal layers: (i) on the top, there is a backfill layer with a thickness ranging between 0.2 and 1 m, where we expect relatively low conductivity and polarization values: (ii) the shallowest geological materials correspond to recent alluvial sediments, mainly gravels and sands extending to maximum depth between 4 and 6 m, which we expect to be related to moderate to low CC values; (iii) a unit of "Hazelnut clay" lenses, composed of sandy-gravelly clays with hazelnut color with a thickness of ca. 1 to 1.5 m, expected to provide a significant increase in the conductivity and polarization due to the

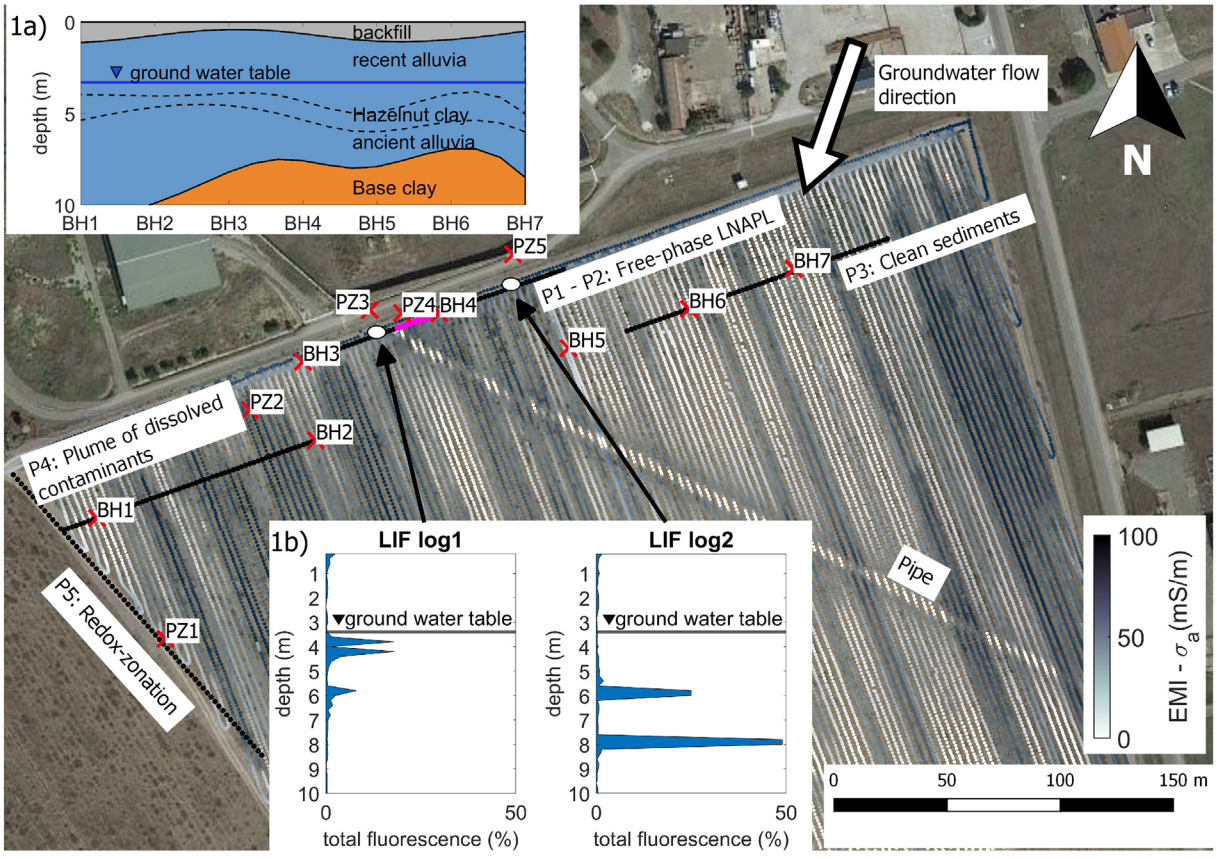

Fig. 1. Orientation of the complex conductivity imaging (CCI) profiles P1 to P5 at the experimental plot in the Decimommanu site. The satellite image indicates the position of the experimental plot in reference to the military air base where the kerosene spills took place. The arrow indicates the direction of the groundwater in the airbase and in the experimental plot. The position of the electrodes for the CCI measurements the two laser induced fluorescence (LIF) loggings is marked with the black and white dots respectively, while the red symbols indicate the position of piezometers and boreholes for the collection of water and soil samples. The map of the apparent conductivity (σ_a) obtained through EMI measurements for a nominal depth of investigation of 6.7 m is imposed on the aerial photography to delineate the presence of infrastructure at the experiment plot. The inserts present: (a) a geological section constructed after the analysis of soil samples recovered after the drilling of 7 boreholes (BH1 to BH7), and (b) variations of the fluorescence measured in the LIF logs. (For interpretation of the references to color in this figure legend, the reader is referred to the web version of this article.)

enhanced surface conductivity; (iv) a layer of ancient alluvial sediments, which extend to a depth between 8 and 11 m, where we expect a higher polarization and conductivity response than the recent alluvia due to its higher content of fine grains; and (v) at the bottom a clay-rich formation which constitutes a lower boundary for groundwater flow where we expect high CC values. The hydrocarbon-contaminants are expected to be found in the alluvial sediments with the characterization of their geophysical response and their extension being the objectives of this study.

Table 1 presents the grain size distribution measured in sediments recovered during the drilling of boreholes. Such analyses demonstrate higher clay content in the ancient (ca. 14%) than the recent (ca. 5%) alluvial sediments; yet, both units are still dominated by gravel and sand content (ca 80%). On the contrary, the Hazelnut clay is mainly composed of fine grains (silt and clay corresponding to more than 60%). The hydraulic conductivity of the different units has been estimated in the range between ~1.8×10^{-4} and 6.5×10^{-6} m/s for the recent alluvial, and between ~1.7×10^{-6} and 1.9×10^{-8} for the ancient alluvial sediments; while the values for the Hazelnut and Base clays have been estimated in the order of 3.4×10^{-9} and 1×10^{-10} m/s respectively. Groundwater flow is found to be predominantly NNE-SSW. During our geophysical survey, the groundwater level in the measurement area was located approximately at 3.30 m below ground surface (bgs).

Remediation of the source zone located within the military station is being monitored by means of a piezometric network consisting of 62 water sampling points. The reported total petroleum hydrocarbon (TPH) and fluid-EC (electrical conductivity) in groundwater samples collected during our campaign in piezometers to the south of the military station are presented in Table 2. The analyses of water samples reveal the highest TPH values (18,000 μg/L) directly at the border of the military station, with a few wells showing relatively high concentrations (TPH between 1200 and 6800 μg/L) extending to the south, in the plume of dissolved contaminants. We also note here that fluid-EC values reveal the lowest values in the hydrocarbon-impacted area (around 1200 μS/cm), while much higher values are reported in the clean area (around 1800 μS/cm). Direct-probe investigations using laser induced fluorescence (LIF) were conducted in 2017 to characterize the extension and thickness of the LNAPL in the military station. The LIF logs measure the fluorescence following the excitation of fluorophores present in jet fuels, permitting a semi-quantitative delineation of LNAPL trapped in the ground (e.g., Lu et al., 2014; García-Rincón et al., 2020). In our study area, information from two LIF logs (see Fig. 1b) are available to aid in the interpretation of the geophysical signatures. At the logging points, the LIF measurements reveal a maximum NAPL thickness of ca 50 cm at depths 5 m bgs. The relatively deep location of the contaminants suggests that the oil was trapped during previous fluctuations of the groundwater table. No hydrocarbons in free-phase have been found further to the south of the military station.

2.2. Geophysical investigation – complex conductivity imaging (CCI) survey

The CCI lines were distributed to cover the different areas of interest: (a) free-phase LNAPL, (b) plume of dispersed contaminants, (c) clean sediments. Line P1 is 94.5 m long (64 electrodes with a separation of 1.5 m between them) and it is centered at the position where two LIF logs have shown the presence of contaminants in free-phase, and TPH in groundwater samples have the highest values (between 1200 and 18,000 μg/L, as presented in Table 2); line P2 is collected in the same position with a smaller separation between electrodes (0.5 m) to gain information with higher resolution at shallower depth. Line P3 represents the control line, collected over clean sediments (no concentration of benzene or THP reported, as presented in Table 2), with the same length as P1, with the three lines oriented in direction E-W. Lines P4 and P5 were collected in the expected plume of dissolved contaminants, in direction E-W and S-N respectively, with a total length of 94.5 and 126 m respectively (1.5 and 2 m separation between electrodes). The position of the electrical lines is shown in Fig. 1. Measurements were collected with a DAS-1 instrument from Multi-Phase Technologies (MPT) at 12 different frequencies between 0.5 Hz and 225 Hz to gain information about the frequency-dependence of the electrical properties in the so-called spectral induced polarization (SIP) or multi-frequency CCI. In each line, measurements were collected with a sequence combining dipole-dipole (DD) and multiple gradient (MG) configurations. The DD configuration is characterized by potential dipoles ahead of the current dipole (to avoid distortions in the data due to the polarization of the electrodes during the current injection); whereas the MG uses small potential dipoles within a larger current dipole. Such articulated configuration aimed at gaining data with high resolution and depth of investigation (favored by DD) as well as high signal-to-noise ratios (S/N favored in MG). Both configurations were designed to include voltage readings with a combination of dipole lengths between 1 and 4 times the electrode spacing (i.e., using skip0 to skip3 configurations, for details see Flores Orozco et al., 2018, 2020) and 8 voltage readings for each current injection (to explore the 8 measuring channels available in the DAS-1). The top soil layer was dry and compact at the time of the survey; thus, we opted to deploy stainless steel (instead of non-polarizable) electrodes hammered in the ground. Contact resistances were always below 1 kΩ for all data sets presented here. All DD measurements were collected as normal and reciprocal pairs to evaluate data quality, where reciprocal refers to the collection of the same quadrupole after interchanging the current and potential dipole (e.g., Flores Orozco et al., 2012b).

The location of the CCI lines was decided taking into account a map of the apparent electrical conductivity (σ_a) gained through measurements with the electromagnetic induction (EMI) method at the low induction number. The EMI map was collected with a CMD-Explorer (from GF instruments), which simultaneously collects readings of the σ_a with three different receivers, for a nominal depth of investigation of 2.3, 4.2, and 6.7 m (in vertical configuration). The EMI map revealed a pipeline crossing the study area with an orientation NW-SE, as presented in Fig. 1. Hence, the position of the CCI lines was selected to avoid the vicinity of the pipeline. Nonetheless, the position of line P1 was fixed due to the LIF logs.

Table 1
Grain size distribution measured in soil samples.

Layer	Sampling depth (m)	Gravel (%)	Sand (%)	Silt (%)	Clay (%)
Recent Alluvial	1.0–3.0	62	26	5	7
	2.0–4.0	55	33	8	4
	1.0–3.0	59	30	5	6
	2.0–4.0	70	23	4	3
Hazelnut clay		14	21	26	39
Ancient Alluvial	7.0–8.0	48	31	8	13
	7.0–8.0	53	26	5	16
	6.0–8.0	56	29	5	10
	6.0–8.0	42	31	9	18

Table 2
Fluid electrical conductivity (Fluid-EC) and concentration of hydrocarbon-contaminants measured in water samples at different sampling points (i.e., boreholes and piezometers) in the study area. The CC line closest to the sampling point is also indicated to help in the comparison with the imaging results.

Sampling point	CC line	Benzene (μg/L)	Ethylbenzene (μg/L)	Styrene (μg/L)	TPH (μg/L)	Fluid EC (μS/cm)
PZ1	P5, P4	0.0011	0	0.15	0	1194
BH7	P3	0	0.015	0.11	0	1860
PZ4	P1	0	0	0	1200	1197
BH5	P3	0	0	0	4700	1312
PZ2	P5, P4	0	0	0	6400	1214
PZ3	P1	0	0	0	6800	1041
PZ6	P1	0	0	0	18,000	1129

All CCI datasets were inverted with CRTomo (by Kemna, 2000), a smoothness-constraint inversion algorithm that solves the Helmhotz equation in the wavenumber domain to calculate the distribution of complex resistivity in a 2D image plane from a set of electrical impedance measurements. CRTomo permits us to control the inversion of the data through the definition of a confidence level determined by the estimated data-error. Quantification of data error in our study was made following the analysis of the misfit between normal and reciprocal measured resistances (described in Flores Orozco et al., 2012b and Flores Orozco et al., 2018). For the data presented here, our analysis estimated a relative error of 5% and an absolute error of 0.01 (Ω) in impedance-magnitude (i.e., resistance) measurements; whereas an absolute error of 3 mrad was found for impedance-phase readings. Inversion results presented here converged all to an error-weighted normalized root mean square (RMS) value of 1 ± 0.02, which indicates that the retrieved electrical model can explain our data in the confidence interval defined by the error model.

3. Results

3.1. The electrical response of clean sediments – line P3

Fig. 2 presents the multi-frequency CCI results of data collected in the clean area of the experimental plot (line P3). These images show the electrical conductivity and induced polarization response expressed in terms of the real (σ') and imaginary (σ'') components of the complex conductivity, as well as in terms of the phase-angle of the complex conductivity (ϕ). Hereafter referred to as phase only, where ϕ values can be approximated as the ratio of the real-to-imaginary component ($\phi \approx \sigma''/\sigma'$) for the low values associated to geophysical measurements (a few tens to hundreds of mrads). Taking into account that both σ' and σ'' are affected by the fluid-EC, the saturation and the porosity, then the phase values might provide a better parameter to evaluate the strength of the polarization effect (e.g., Slater and Lesmes, 2002). We also note here that the real component of the complex conductivity (σ') is also commonly referred to as the electrical conductivity, bulk conductivity or direct-current conductivity (DC-conductivity), which is solved through commonly used electrical resistivity tomography (ERT).

Fig. 2 shows the presence of four main layers in accordance with the expected geology at the site. The top layer corresponds to the backfill material and the unsaturated sediments exhibiting the lowest electrical response (in both conductivity and polarization), with the lowest polarization values observed for the backfill materials. Such low complex conductivity values are expected for dry materials with low specific surface area, where current cannot easily flow and the limited presence of dissolved ions results in negligible polarization of the EDL. The second layer corresponds to the saturated recent alluvia sediments, related to moderate values of the electrical conductivity and polarization (σ' ~20 mS/m and σ'' ~0.8 mS/m). The third layer corresponds to the highest σ' and σ'' values associated to the ancient alluvia sediments, with the increase in both parameters explained by surface conduction explained by the increase in the clay content clay content (e.g., Slater and Lesmes, 2002; Flores Orozco et al., 2018). The images of the σ' reveal a perfect agreement with the location of the groundwater table, with a significant increase in the electrical conductivity from dry to saturated sediments (from values ca. 1 to 10 mS/m), as well as a clear contact with the more conductive materials from the ancient alluvial at ca. 5 m bgs. A better discrimination of the different units can be observed in the images of the polarization effect (σ''). Fig. 2 reveals the lowest values ($\sigma'' < 0.01$ mS/m) resolved for the shallowest backfill materials (within the surface and 2 m bgs), and intermediate values corresponding to the

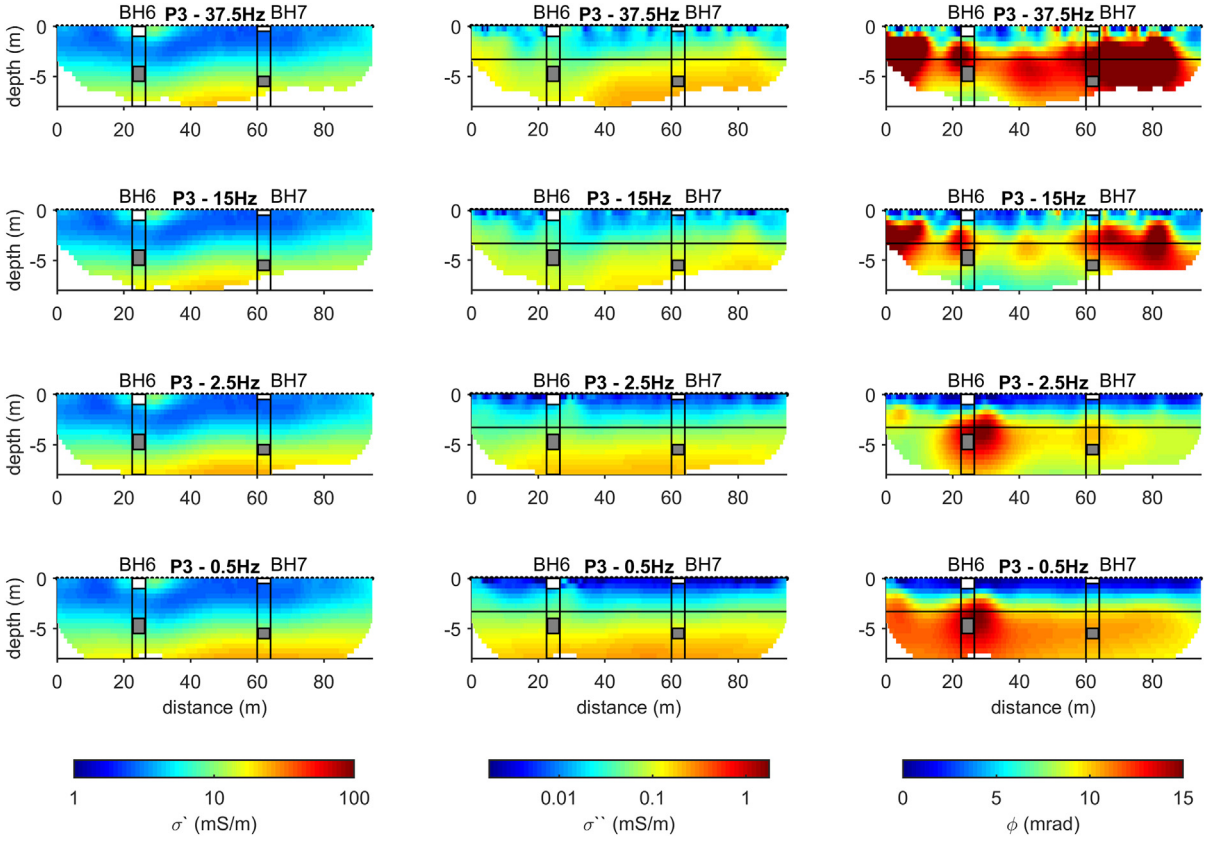

Fig. 2. CCI results for data collected along the clean sediments along line P3 expressed in terms of the real, imaginary and phase of the complex conductivity, for data collected at different acquisition frequencies. The dots at the surface show the position of the electrodes, while the continuous horizontal line at 3.3 m depth indicates the position of the groundwater table during our measurements. Lithological information obtained from boreholes BH6 and BH7 is imposed on the electrical model, with the boxes, indicating: the backfill materials on the top (white), the recent alluvial (no color), the Hazelnut clays (gray) and the ancient alluvial sediments (no color).

recent alluvia sediments, extending above the position of the groundwater table to the contact with the Hazelnut clays around 4.5 m depth. The higher polarization values (σ'' ~ 0.5 mS/m) can be observed for the Hazelnut clays and the ancient alluvia sediments. The Base clay is found at depth below 8 m bgs and cannot be observed in Fig. 2. The high σ'' values observed above the water table (in the recent alluvia) can be explained considering that the thickness of the EDL is about a few tens of nanometers (see Bohinc et al., 2001 and references therein); thus, the pore space does not need to be fully saturated to permit a polarization response. Accordingly, a thin water film surrounding the sediments might still permit polarization effects even if they are not fully saturated (as observed in laboratory studies, for instance Breede et al., 2012). The increase in the polarization response (σ'') in the Hazelnut clays and ancient alluvia sediments is consistent with their relatively high clay content as presented in Table 1. Expressed in terms of the phase, the polarization images reveal larger variability, with values in the range between 5 and 15 mrads. Variations in the content of coarse and fine sediments (see Table 1) can explain the relatively variability in phase values observed in Fig. 2. Possible inferences of anthropogenic structures in the anomaly located between 20 and 30 m along profile P3 can be disregarded, considering that the EMI data did not reveal any particular feature at this position. Thus, we interpret an increase in the fine content, as the parameter controlling the increase of ϕ values. The increase in the values at high frequencies (i.e., above 10 Hz) also confirms the polarization of the fine fraction, which is expected at high frequencies (e.g., Revil and Florsch, 2010; Breede et al., 2012; Bücker et al., 2019). Nonetheless, at such frequencies it is not possible to neglect potential distortions in the polarization measurements due to undesired electromagnetic (EM) fields, commonly referred to as EM coupling (e.g., Hallof, 1974, and Flores Orozco et al., 2018; Zimmermann et al., 2019; Flores Orozco et al., 2020 and references therein). Hence, the increase in the phase observed at 15 and 37.5 Hz cannot be only interpreted as the response related to clay minerals (e.g., Slater and Lesmes, 2002; Breede et al., 2012; Bücker et al., 2019), but a superposition with possible EM effects.

3.2. The electrical response of sediments impacted with free-phase LNAPL – line P1

In Fig. 3 we present the imaging results for data collected along line P1, where two LIF logs are available for the interpretation of the electrical signatures (at 45 and 80 m along P1). In agreement with the imaging results for the control line, Fig. 3 also reveals three layers, with the top layer related to the lowest σ' and σ'' values above the groundwater table and the second layer corresponding to the saturated materials corresponding to higher σ' and σ'' values. The third layer, corresponding to the Hazelnut clays and ancient alluvia sediments, reveals high values which are consistent (σ' ~80 and σ'' ~0.8 mS/m) to those resolved for line P3; however, the contact to this layer is found at a depth of ca. 5 m, corresponding to ~1 m shallower than in line P3. LIF revealed peaks with 20% fluorescence at 4 and 6 m bgs in LIF log 1, and 25% was observed at 6 m bgs in LIF log 2, while the highest values (50% fluorescence) were observed in LIF log2 at 8 m depth. Interpretation of the LIF data at the site delineates LNAPL in free phase as a continuous layer of ~50 cm thickness. However, such interpretation cannot be supported with CCI presented in Fig. 3.

Similar to the control line, the lowest σ'' values (<0.01 mS/m) correspond to the backfill and the recent alluvia sediments (compacted and dry), whereas moderate values are resolved around the groundwater table (~0.08 mS/m) and the highest values in the Hazelnut clays and the ancient alluvia. Recently, the studies by Mewafy et al. (2013) and Abdel Aal et al. (2014) suggested that accumulation of iron sulfides (an electrical semi-conductor) could explain an increase in the complex conductivity, especially evidenced by an increase in the polarization effect. At the field scale, CCI results, also in alluvial sediments, revealed a significant increase in the polarization response accompanying the stimulation of iron reducing-bacteria during bioremediation of a uranium-contaminated site (e.g., Flores Orozco et al., 2011, 2013). However, analyses of the sediments during the excavation of boreholes BH1 to BH7 did not reveal any change that could point to the accumulation of iron sulfides; thus, we cannot use the arguments pointed out in the studies by Mewafy et al. (2013) and Abdel Aal et al. (2014). Nonetheless, the slight increase in the complex conductivity could be related to changes in the wettability of the compound, due to the chemical transformations of the contaminant as a consequence of possible biosurfactants (e.g., Cassidy et al., 2001). The increase in the real and imaginary components of the CC due to oil-wetting oils has been reported in laboratory studies (Revil et al., 2011; Abdel Aal and Atekwana, 2014).

Fig. 3 shows a significant decrease in ϕ for those locations where the LIF revealed the presence of free-phase LNAPL, in accordance with previous studies investigating non-polar compounds in the laboratory (e.g., Ustra et al., 2012) and at the field scale (e.g., Flores Orozco et al., 2012a, 2019b). The anomalous regions show lower ϕ values than those observed in the clean sediments (line P3), clearly indicating the sensitivity of the CCI to delineate subsurface variations imposed by the LNPAL in free-phase. The free-phase found by LIF data shows up in disconnected regions in the deeper position of the profile, below the water table; thus, these anomalies are likely to be related to trapped hydrocarbons, which cannot any longer move up and down together with the groundwater level.

Additionally, Fig. 3 also reveals a weak frequency-dependence in the complex conductivity, with σ'' and ϕ values exhibiting only small variations for data collected at different frequencies. Similar to the results observed for line P3 (Fig. 2), the highest response is observed at 0.5 Hz, with a decrease in the values towards 15 Hz, yet a larger increase in σ'' and ϕ can be observed at 37.5 Hz, likely indicating the polarization of the fine grains and possible distortions in the data due to EM effects.

3.3. The plume of dissolved contaminants – line P4

Line P4 was collected in areas where direct measurements on groundwater samples reveal total petroleum hydrocarbons (TPH) values around 500 μg/L (Table 2), corresponding to a plume of dissolved contaminants. Fig. 4 shows the electrical images for line P4, which yield a magnitude and distribution of the complex conductivity parameters (σ', σ'' and ϕ) consistent to those of lines P1 (Fig. 3) and P3 (Fig. 2), yet some differences can be identified. We can still interpret the three layers model defined by unsaturated sediments, the saturated ones and the Hazelnut clays and ancient alluvia at the bottom. Although the backfill and unsaturated alluvia sediments reveal consistently low σ'' values (<0.01 mS/m), this layer exhibits higher electrical conductivity values ($\sigma' > 15$ mS/m) than those observed in lines P1 and P3. Moreover, the saturated aluvia sediments show higher values for both σ' and σ'' than those observed in lines P1 and P3. This is a clue that some other subsurface phenomena, in addition to geological contrasts, controls the electrical conductivity distribution in the shallow subsurface at the position of line P4.

Measurements at high frequencies (>37.5 Hz) reveal in general an increase in the polarization response resulting from the polarization of the fine fraction, and possible inductive EM effects in the data. Lateral variations in the electrical properties presented in Fig. 4 can be related to the variations in fine fractions of the Hazelnut clays and ancient alluvial sediments, as observed in the alluvia sediments reported in Table 1.

4. Discussions

4.1. Comparison of electrical signatures: data collected in clean and hydrocarbon-impacted sediments

For a quantitative comparison of the electrical signatures at low frequencies, we present in Fig. 5 the σ'' values plotted against the σ' for

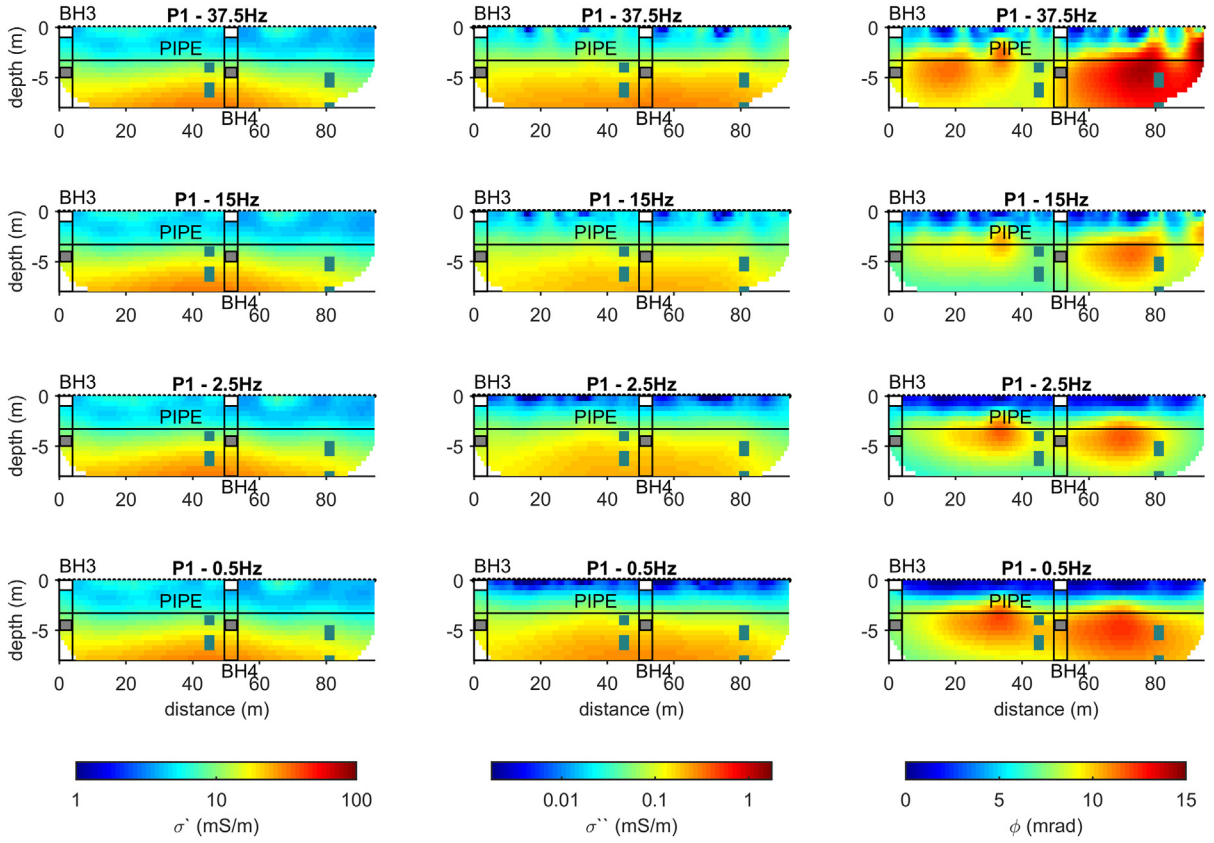

Fig. 3. CCI results for data collected along profile P1 where the presence of LNAPL in free-phase has been reported by means of LIF logging (indicated by the blue rectangles at ca. 45 and 80 m of the profile distance). The CCI are presented in terms of the real, imaginary and phase of the complex conductivity. The dots at the surface show the position of the electrodes, while the continuous horizontal line at 3.3 m depth indicates the position of the groundwater table during our measurements. Lithological information obtained from boreholes BH6 and BH7 is imposed on the electrical model, with the boxes, indicating: the backfill materials on the top (white), the recent alluvial (no color), the Hazelnut clays (gray) and the ancient alluvial sediments (no color). (For interpretation of the references to color in this figure legend, the reader is referred to the web version of this article.)

pixel values extracted from the imaging results for lines P1 (representing the LNAPL in free-phase), P2 (clean sediments) and P4 (plume of dissolved contaminants) but sorted in three regions: unsaturated sediments (between 1 and 2 m bgs), around the water table where the LNAPL is expected (between 2.80 and 3.80 m bgs) and in the saturated sediments (between 4.5 and 5.5 m bgs). Fig. 5 reveals some clear features, namely: (Abdel Aal and Atekwana, 2014) electrical parameters for the contaminated sediments are higher than those in clean sediments, and (Abdel Aal et al., 2014) an increase in the electrical properties with increasing frequency. As discussed above, the increase in the σ'' with increasing the frequency is related to the polarization of the fine fraction, associated to fast polarization processes, captured at frequencies above 100 Hz (e.g., Slater and Lesmes, 2002; Revil and Florsch, 2010; Binley et al., 2015; Osterman et al., 2019); although a possible superposition of EM inductive coupling and Maxwell-Wagner polarization effects cannot be neglected. Nonetheless, Fig. 5 reveals consistent patterns in the electrical properties (σ' and σ'') for changes in the concentration of LNAPL in the subsurface, with such variations observed for all frequencies investigated here (between 0.5 and 37.5 Hz).

The lowest σ' and σ'' values correspond to backfill materials and the unsaturated recent alluvial sediments. This is as expected, considering that the EDL can only be formed at the grain-fluid interface, which might not be developed in dry sediments. Yet among these, the highest values correspond to those retrieved from the dissolved plume of contaminants. Although σ'' values are two orders of magnitude smaller than σ', unconsolidated sediments at low frequencies (0.125 and 1 Hz) reveal a bulk conductivity (in the range σ' between 5 and 10 mS/m) much larger than the polarization (σ'' between 0.025 and 0.05 mS/m). Based on such variation, we conclude that electrolytic conduction dominates over surface conduction. In case of the unsaturated materials, our results reveal consistency with previous laboratory studies which also have observed an increase in the electrical conductivity (σ') when increasing the volumetric content of non-polar compounds (Schwartz et al., 2012; Shefer et al., 2013). Likewise in the saturated zone, our results are consistent with the laboratory studies which have reported an increase in σ'' with increasing the volumetric content of non-polar compounds (e.g., Schmutz et al., 2010; Blondel et al., 2014). Similar to the study by Blondel et al. (2014), we observed at the field scale an increase in the electrical conductivity (σ') in apparent contradiction with lab studies. Taking into account the relatively low TPH concentrations measured in water samples (Table 2) in our study, we interpret such increase in both σ' and σ'' due to enhanced surface conductivity following the enrichment of charges at the EDL due to the presence of non-miscible oils in the pore water. Such increase in both components of the CC for low concentration of non-wetting compounds has also been predicted by the model by Bücker et al. (2017). Moreover, we cannot disregard the possibility that the wettability of such oils have changed their polarity and act as wetting-oils, which cause an increase in σ'' (e.g., Revil et al., 2011: Abdel Aal and Atekwana, 2014). Accordingly, the simultaneous increase in σ' and σ'' results in the low ϕ values in saturated materials in the dissolved plume observed in Fig. 4. However, contrary to the study by Schmutz et al. (2010), in our study we observe the lowest polarization values (both σ'' and ϕ) resolved for the saturated areas where LIF data indicate the presence of free-phase LNAPL.

The increase of electrical conductivity observed in the contaminated areas can be explained by the adsorption of the NAPL into the grain

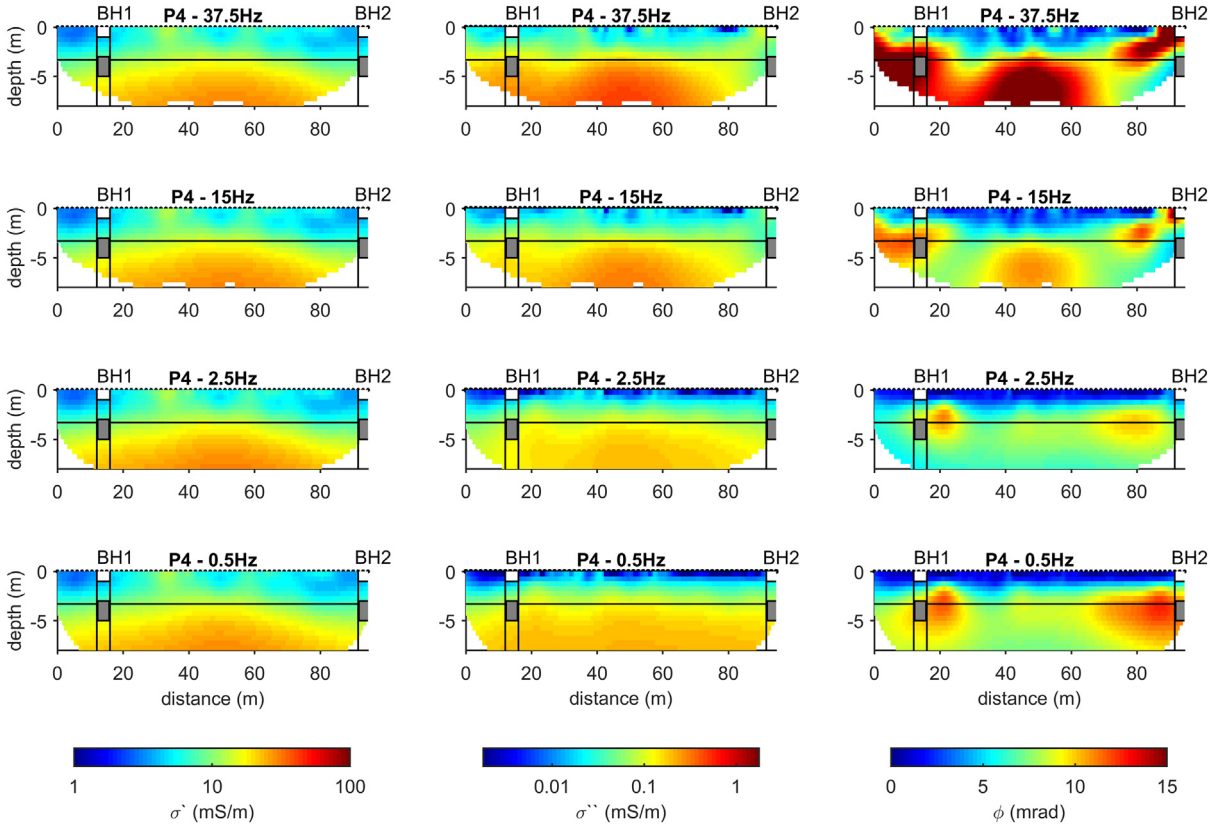

Fig. 4. CCI results for data collected along the expected position of the plume of contaminants (line P4). The electrical response is expressed in terms of the real, imaginary and phase of the complex conductivity at different frequencies. The dots at the surface show the position of the electrodes, while the continuous horizontal line at 3.3 m depth indicates the position of the groundwater table during our measurements. Lithological information obtained from boreholes BH6 and BH7 is imposed on the electrical model, with the boxes, indicating: the backfill materials on the top (white), the recent alluvial (no color), the Hazelnut clays (gray) and the ancient alluvial sediments (no color).

surface (e.g., Schwartz et al., 2012) or by the accumulation of metabolic products accompanying the stimulation of microbial activity, as observed in numerous studies (e.g., Abdel Aal et al., 2006, 2014; Atekwana and Atekwana, 2010; Cassiani et al., 2014; Flores Orozco et al., 2012a, 2019a, 2019b; Mewafy et al., 2013). Microbial transformation of hydrocarbon contaminants results in the formation of a redox zonation following a respiration pathway, the sequence of which depends on the potential energy yield (Löser et al., 1998; Kłonowski et al., 2008). In particular: aerobic respiration, denitrification, manganese reduction, iron reduction, sulphate reduction, and metanogenesis proceed in decreasing order of energy efficiency, with different bacterial strains taking advantage of the relevant electron acceptors. Accumulation of metabolic products could also explain why the conductivity values in the sediments impacted by NAPL in free-phase show a higher conductivity than those in the clean area. However, analyses of groundwater samples reveal that fluid-EC values in samples collected from clean areas (between 1200 and 1800 μS/cm) are higher than in those samples collected around P1 (values between 1000 and 1200 μS/cm). The higher fluid-EC values reported in clean areas might not support the accumulation of metabolic products. Hence, we hypothesize that the increase in the polarization response could be related to changes in the wettability of the jet fuel following hydrocarbon degradation and the activity of surfactants at the site (e.g., Cassidy et al., 2001). Although we lack evidence about this, the presence of polar compounds (i.e., oil-wetting the grain surfaces) results in an increase in the σ'', in agreement with the patterns observed in Fig. 5.

Fuel hydrocarbons are LNAPL and, thus, are expected to float on top of the water table. Yet, it is well known (e.g. Cassiani et al., 2014) that water table fluctuations inevitably trap free phase hydrocarbon as a residual phase in the so-called smearing zone. Hence, plots in Fig. 5 aimed at comparing the electrical response around the water table with the one related to the saturated zone are very instructive. In general, it is possible to observe that both regions have similar distribution, with σ' and σ'' values laying along a linear model ($\sigma' \sim 100\sigma''$). The increase in both conductivity and polarization indicates that in these regions surface conductivity dominates over electrolytic conductivity. Hence, it is the polarization of the EDL that controls the electrical response for the sediments extending below 2 m depth down to the contact with the Hazelnut clays. The only difference observed is that the response around the water table is ca 30% lower than the one related to the saturated materials. Similar to the trend observed for unsaturated materials, higher values are also observed for the plume of dissolved contaminants, while the clean sediments show the lowest response for both σ' and σ''. The increase of both the electrical conductivity and the induced polarization can be explained by the addition of charges from the bulk electrolyte into the EDL associated to the presence of immiscible oils in pore water (e.g., Bücker et al., 2017). As discussed above, the increase in the fluid conductivity due to the biotic (or abiotic) transformation of the fuel and the weathering of grains cannot be sustained in our study considering that fluid-EC in groundwater samples from clean sediments is higher than those collected in the plume of contaminant. Nonetheless, changes in the wettability of the oil cannot be disregarded, which could provide a simple explanation on the observed increase in the polarization response for hydrocarbon-impacted sediments, as observed in previous laboratory studies (e.g., Revil et al., 2011; Abdel Aal and Atekwana, 2014).

4.2. Improved interpretation of jet fuel spills by combination of fluorescence logs and complex conductivity imaging

Comparison of the CCI results collected at different locations of the study area cannot sustain the interpretation of a contaminant continuous

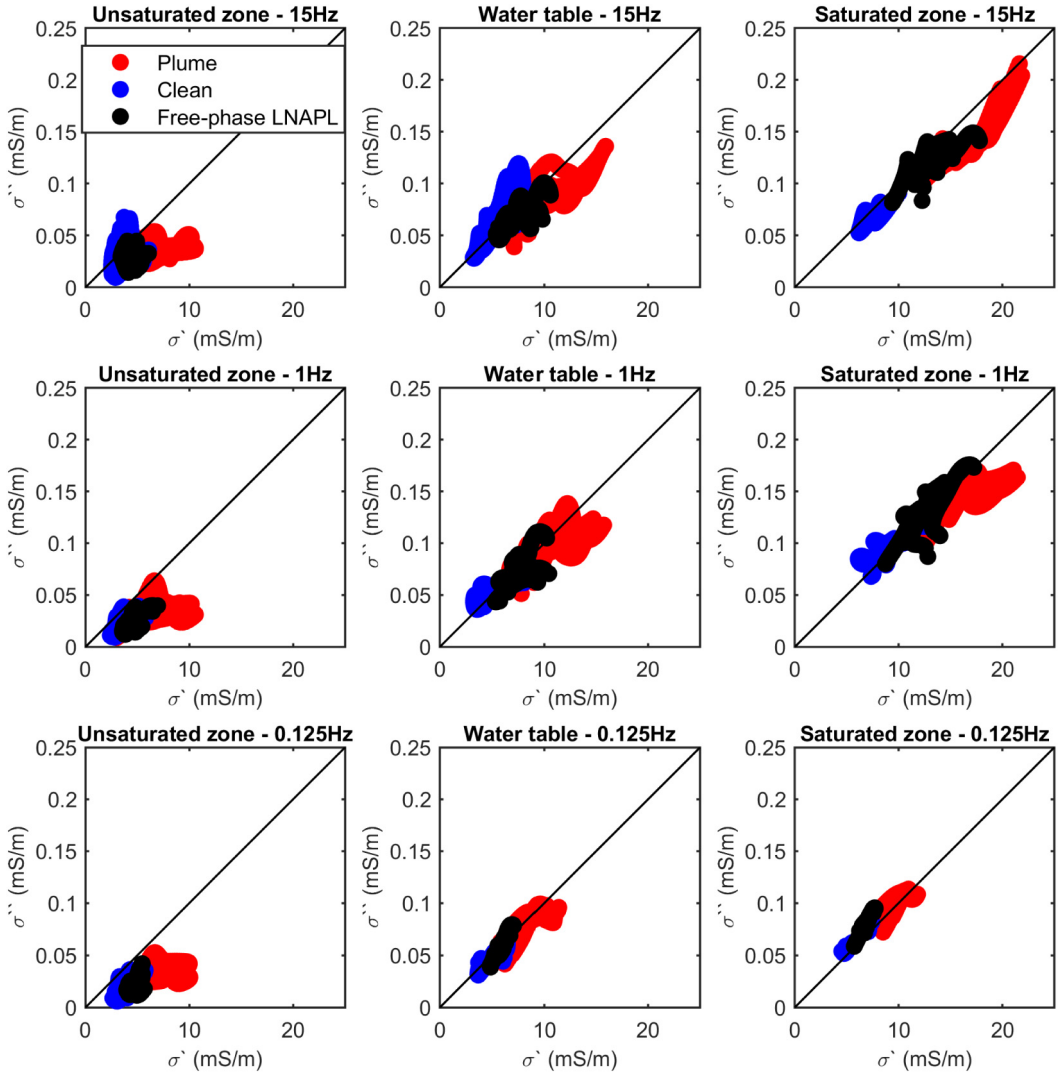

Fig. 5. Correlation of the electrical conductivity and induced polarization properties of the subsurface, expressed in terms of the real (σ') and imaginary (σ'') component of the complex conductivity. The plots show pixel values extracted from the CCI results extracted at different depth: between 1 and 2 m (in the unsaturated zone), between 2.80 and 3.80 (around the water table), and between 4.5 and 5.5 (in the saturated materials). Electrical parameters are extracted from the different areas: clean sediments (corresponding to P3), around the areas where LNAPL has been detected in free-phase (P1) and in the plume of dissolved contaminants (P4). The black line indicates a linear increase related to the model $\sigma' = 100\sigma''$, which is used to indicate regions dominated by electrolytic conduction (below line) and surface conduction (along the line).

layer between LIF logging points 1 and 2 located along line P1. This is the main limitation of direct methods: though they provide direct measurements of the contaminants, the information is limited to the sampling location or logging profile. Hence, the joint interpretation of direct measurements and geophysical surveys permits to obtain a better image of the site's conditions. Based on the interpretation of both CCI and LIF results, it is possible to suggest that the LNPAL moved down-gradient from the source zone near the fuel tanks along preferential pathways which can be observed in the two points spotted by the LIF logging. Such points are related to low σ' and σ'' values, while the soil material between them shows higher conductivity and polarization response at the same time. Thus, CCI indicates that such points are not connected by a continuous contaminant plume. Moreover, the electrical survey results for areas affected by the plume of dissolved contaminants (line P4) show much higher σ' and σ'' values than those between the LIF logs, suggesting that the kerosene in free-phase is not extended down-gradient from the position of line P1, but towards the location of P4 and P5. The highest fluorescence values (>20%) are observed below the water table, in discrete positions, supporting the interpretation that these points are not connected as a continuous free-phase contaminant, but likely represent an immobile residual fraction of the jet fuel. Moreover, the highest fluorescence (>40% in the LIF log2 presented in Fig. 1) is found at the depth corresponding to the Hazelnut clay; this supports our interpretation that these contaminants refer to an immobile phase trapped within soils with high content in fine fractions. Changes in pore-space geometry due to oil droplets trapped within the micro pores has been suggested as an explanation of the sudden drop in the polarization response in CC measurements (see Bücker et al., 2017). However, this model predicts that the free-phase is connecting both large and small pores, which cannot be expected for the spatially constraint spots in our study. Hence, we suggest that the free-phase contaminants are trapped within sediments rich in fine fractions, related to smaller pore throats (e.g., Binley et al., 2015). Accordingly, the free-phase contaminant is likely connecting a series of small pores resulting in the decrease of the polarization response, in agreement with the model proposed by Bücker et al. (2017).

Although CCI permits to solve for quasi-continuous information about subsurface properties, the interpretation of the electrical properties is unfeasible without geochemical information, for instance, contaminant concentrations and grain size distribution. The sensitivity of the electrical signatures to textural parameters of the soil (e.g., Revil and Florsch, 2010; Binley et al., 2015; Bücker et al., 2019), NAPL

concentrations (e.g., Cassiani et al., 2009; Schwartz et al., 2012; Shefer et al., 2013) as well as to chemical parameters of groundwater such as salinity, pH, and wettability of NAPL (e.g., Hördt et al., 2016; Revil et al., 2011; Bücker et al., 2017) make the postulation of a universal law for the interpretation of CC signatures almost impossible. The interpretation of CC signatures at the field scale becomes more challenging when biogeochemical transformations of the hydrocarbon and the matrix are taken into account (e.g., Abdel Aal et al., 2006, 2014; Atekwana and Atekwana, 2010; Mewafy et al., 2013). In particular, the application of the CCI method requires of analyses to assess the wettability of the hydrocarbon-contaminants, as this parameters play a dominant role in the actual electrical properties (e.g., Revil et al., 2011; Schwartz et al., 2012; Shefer et al., 2013; Abdel Aal and Atekwana, 2014). Hence, the collection of data through direct methods is critical for a quantitative interpretation of the geophysical results. Additionally, geophysical results could be used to select the location for the collection of soil and water samples, rendering both a cost-effective investigation of contaminated sites and fully exploit the high spatial resolution from geophysical results.

Regarding the conduction of CC (or IP) surveys, to date inversion algorithms (e.g., Fiandaca et al., 2013) also permit to solve for the frequency-dependence of the electrical properties based on measurement of the full-wave form in direct-current (DC) instruments; thus, reducing acquisition time by avoiding the repetition of the measurements at different frequencies. However, in this study we aimed at gaining information about the actual frequency-dependence in the data and the comparison of field and laboratory signatures. Such information may help to understand the controls of the electrical properties in hydrocarbon-impacted areas at the field-scale and exploit the full potential of the CC method, which could be also used to gain information about hydraulic properties of the subsurface (e.g., Kemna et al., 2004; Maurya et al., 2018; Revil and Florsch, 2010). Such information might be relevant for the delineation of preferential flow paths for contaminant. Fig. 5 presents a simple way to visualize changes in the CC associated to different concentrations of hydrocarbon-contaminants in groundwater. As discussed before, such variations are consistent with laboratory observations, yet might be site-specific. Accordingly, further field investigations are required to better understand the controls of the IP response, in particular, to discriminate between textural information, hydrocarbon concentration and possible biogeochemical transformations of the pore-space.

5. Conclusions

Our study demonstrates that the combination of direct investigations and geophysical results, the latter obtained by means of the complex conductivity imaging (CCI) method, can significantly improve a site's conceptual model in terms of hydrocarbon contaminant distribution. In particular, in our study we demonstrate that the interpretation of interpolated LIF logs as a continuous LNAPL contaminant might not be accurate because of inadequate spatial sampling. Interpretation of CCI results alone, without the LIF data, would also be impossible, considering that different chemical and textural parameters control textural and chemical the electrical response of contaminated soils. However, a combination of both the CCI and the LIF data provides a better understanding of subsurface properties and the architecture of contaminant plumes. Hence, we interpret the anomalous regions along line P1 characterized by low ϕ values as two points where kerosene is trapped in free-phase, resulting in anomalous values with high fluorescence in LIF logs.

Although the exact values on the volumetric content of kerosene are not known in the area under investigation, the comparison of CCI results collected at different locations allows us to delineate a clear pattern in the electrical properties regarding the extension of the mature kerosene contaminant plume: the lowest σ' and σ'' are related to clean sediments, whereas the highest values indicate areas affected by the dissolved plume of contaminants. This increase can be explained by two main mechanisms: (i) the disconnection of the electrical double layer due to the presence of immiscible oils in the pores; and (ii) the increase of ions from the bulk electrolyte into the electrical double layer associated to the presence of the non-miscible oils in the pore water. The observed increase in the electrical properties for hydrocarbon-impacted sediments also suggests changes in the wettability of the contaminant, with oil-wetting (i.e., polar) compounds commonly related to similar responses to those observed in our study.

CRediT authorship contribution statement

Adrián Flores Orozco: Conceptualization, Methodology, Software, Formal analysis, Investigation, Data curation, Writing - original draft, Visualization, Supervision, Project administration. **Paolo Ciampi:** Methodology, Validation, Formal analysis, Resources, Writing - review & editing, Visualization. **Timea Katona:** Methodology, Validation, Formal analysis, Resources, Writing - review & editing, Visualization. **Matteo Censini:** Methodology, Validation, Formal analysis, Resources, Writing - review & editing, Visualization. **Marco Petrangeli Papini:** Methodology, Validation, Formal analysis, Resources, Writing - review & editing, Supervision, Project administration, Funding acquisition. **Gian Piero Deidda:** Methodology, Validation, Formal analysis, Resources, Writing - review & editing, Supervision, Project administration, Funding acquisition. **Giorgio Cassiani:** Methodology, Validation, Formal analysis, Resources, Writing – review & editing, Supervision, Project administration, Funding acquisition.

Declaration of competing interest

The authors declare that they have no known competing financial interests or personal relationships that could have appeared to influence the work reported in this paper.

Acknowledgments

We gratefully acknowledge the financial support provided by the Italian Ministry of Foreign Affairs and International Cooperation, within the Cooperation Agreement for Science, Technology and Industry between Italy and Israel (2017 call), project “GEOCONS – GEOphysical methods for the characterization of CONtaminated Sites”. We thank the comments of two anonymous reviewers and the Associate Editor for their comments that helped to improve the quality of this manuscript.

References

Abdel Aal, G.Z., Atekwana, E.A., 2014. Spectral induced polarization (SIP) response of biodegraded oil in porous media. Geophys. J. Int. 196 (2), 804–817.

Abdel Aal, G.Z., Slater, L.D., Atekwana, E.A., 2006. Induced-polarization measurements on unconsolidated sediments from a site of active hydrocarbon biodegradation. Geophysics 71 (2), H13–H24.

Abdel Aal, G.Z., Atekwana, E.A., Revil, A., 2014. Geophysical signatures of disseminated iron minerals: a proxy for understanding subsurface biophysicochemical processes. Journal of Geophysical Research: Biogeosciences 119 (9), 1831–1849.

Algreen, M., Kalisz, M., Stalder, M., Martac, E., Krupanek, J., Trapp, S., Bartke, S., 2015. Using pre-screening methods for an effective and reliable site characterization at megasites. Environ. Sci. Pollut. Res. 22 (19), 14673–14686.

Atekwana, E.A., Atekwana, E.A., 2010. Geophysical signatures of microbial activity at hydrocarbon contaminated sites: a review. Surv. Geophys. 31 (2), 247–283.

Atekwana, E.A., Slater, L.D., 2009. Biogeophysics: a new frontier in earth science research. Rev. Geophys. 47 (4).

Atekwana, E.A., Atekwana, E.A., Werkema, D.D., Allen, J.P., Smart, L.A., Duris, J.W., Cassidy, D.P., Sauck, W.A., Rossbach, S., 2004. Evidence for microbial enhanced electrical conductivity in hydrocarbon-contaminated sediments. Geophys. Res. Lett. 31 (23).

Bennett, B., Buckman, J.O., Bowler, B.F.J., Larter, S.R., 2004. Wettability alteration in petroleum systems: the role of polar non-hydrocarbons. Pet. Geosci. 10 (3), 271–277.

Binley, A., Hubbard, S.S., Huisman, J.A., Revil, A., Robinson, D.A., Singha, K., Slater, L.D., 2015. The emergence of hydrogeophysics for improved understanding of subsurface processes over multiple scales. Water Resour. Res. 51 (6), 3837–3866.

Blondel, A., Schmutz, M., Franceschi, M., Tichané, F., Carles, M., 2014. Temporal evolution of the geoelectrical response on a hydrocarbon contaminated site. J. Appl. Geophys. 103, 161–171.
Bohinc, K., Kralj-Iglič, V., Iglič, A., 2001. Thickness of electrical double layer. Effect of ion size. Electrochim. Acta 46 (19), 3033–3040.
Breede, K., Kemna, A., Esser, O., Zimmermann, E., Vereecken, H., Huisman, J.A., 2012. Spectral induced polarization measurements on variably saturated sand-clay mixtures. Near Surface Geophysics 10 (6), 479–489.
Bücker, M., Flores Orozco, A., Hördt, A., Kemna, A., 2017. An analytical membrane-polarization model to predict the complex conductivity signature of immiscible liquid hydrocarbon contaminants. Near Surface Geophysics 15 (6), 547–562.
Bücker, M., Flores Orozco, A., Undorf, S., Kemna, A., 2019. On the Role of Stern-and Diffuse-Layer Polarization Mechanisms in Porous Media. Journal of Geophysical Research: Solid Earth 124 (6), 5656–5677.
Cassiani, G., Kemna, A., Villa, A., Zimmermann, E., 2009. Spectral induced polarization for the characterization of free-phase hydrocarbon contamination of sediments with low clay content. Near Surface Geophysics 7 (5–6), 547–562.
Cassiani, G., Binley, A., Kemna, A., Wehrer, M., Flores Orozco, A., Deiana, R., Boaga, J., Rossi, M., Dietrich, P., Werban, U., Zschornack, L., 2014. Noninvasive characterization of the Trecate (Italy) crude-oil contaminated site: links between contamination and geophysical signals. Environ. Sci. Pollut. Res. 21 (15), 8914–8931.
Cassidy, D.P., Werkema Jr., D.D., Sauck, W., Atekwana, E., Rossbach, S., Duris, J., 2001. The effects of LNAPL biodegradation products on electrical conductivity measurements. Journal of Environmental & Engineering Geophysics 6 (1), 47–52.
Caterina, D., Flores Orozco, A., Nguyen, F., 2017. Long-term ERT monitoring of biogeochemical changes of an aged hydrocarbon contamination. J. Contam. Hydrol. 201, 19–29.
Chambers, J.E., Wilkinson, P.B., Wealthall, G.P., Loke, M.H., Dearden, R., Wilson, R., Allen, D., Ogilvy, R.D., 2010. Hydrogeophysical imaging of deposit heterogeneity and groundwater chemistry changes during DNAPL source zone bioremediation. J. Contam. Hydrol. 118 (1–2), 43–61.
Che-Alota, V., Atekwana, E.A., Atekwana, E.A., Sauck, W.A., Werkema Jr., D.D., 2009. Temporal geophysical signatures from contaminant-mass remediation. Geophysics 74 (4), B113–B123.
Deceuster, J., Kaufmann, O., 2012. Improving the delineation of hydrocarbon-impacted soils and water through induced polarization (IP) tomographies: a field study at an industrial waste land. J. Contam. Hydrol. 136, 25–42.
Fiandaca, G., Ramm, J., Binley, A., Gazoty, A., Christiansen, A.V., Auken, E., 2013. Resolving spectral information from time domain induced polarization data through 2-D inversion. Geophys. J. Int. 192 (2), 631–646.
Flores Orozco, A., Williams, K.H., Long, P.E., Hubbard, S.S., Kemna, A., 2011. Using complex resistivity imaging to infer biogeochemical processes associated with bioremediation of an uranium-contaminated aquifer. Journal of Geophysical Research: Biogeosciences 116 (G3).
Flores Orozco, A., Kemna, A., Oberdörster, C., Zschornack, L., Leven, C., Dietrich, P., Weiss, H., 2012a. Delineation of subsurface hydrocarbon contamination at a former hydrogenation plant using spectral induced polarization imaging. J. Contam. Hydrol. 136, 131–144.
Flores Orozco, A., Kemna, A., Zimmermann, E., 2012b. Data error quantification in spectral induced polarization imaging. Geophysics 77 (3), E227–E237.
Flores Orozco, A., Williams, K.H., Kemna, A., 2013. Time-lapse spectral induced polarization imaging of stimulated uranium bioremediation. Near Surface Geophysics 11 (5), 531–544.
Flores Orozco, A., Velimirovic, M., Tosco, T., Kemna, A., Sapion, H., Klaas, N., Sethi, R., Bastiaens, L., 2015. Monitoring the injection of microscale zerovalent iron particles for groundwater remediation by means of complex electrical conductivity imaging. Environmental Science & Technology 49 (9), 5593–5600.
Flores Orozco, A., Bücker, M., Steiner, M., Malet, J.P., 2018. Complex-conductivity imaging for the understanding of landslide architecture. Eng. Geol. 243, 241–252.
Flores Orozco, A., Micić, V., Bücker, M., Gallistl, J., Hofmann, T., Nguyen, F., 2019a. Complex-conductivity monitoring to delineate aquifer pore clogging during nanoparticles injection. Geophys. J. Int. 218 (3), 1838–1852.
Flores Orozco, A., Kemna, A., Binley, A., Cassiani, G., 2019b. Analysis of time-lapse data error in complex conductivity imaging to alleviate anthropogenic noise for site characterization. Geophysics 84 (2), B181–B193.
Flores Orozco, A., Gallistl, J., Steiner, M., Brandstätter, C., Fellner, J., 2020. Mapping biogeochemically active zones in landfills with induced polarization imaging: the Heferlbach landfill. Waste Manag. 107, 121–132.
García-Rincón, J., Gatsios, E., Rayner, J.L., McLaughlan, R.G., Davis, G.B., 2020. Laser-Induced Fluorescence Logging as a High-Resolution Characterisation Tool to Assess LNAPL Mobility. Science of The Total Environment, p. 138480.
Haagh, M.E.J., Schilderink, N., Duits, M.H.G., Siretanu, I., Krawiec, P., Collins, I.R., Mugele, F., 2020. Aging brine-dependent deposition of crude oil components onto mica substrates, and its consequences for wettability. Fuel 274, 117856.
Hallof, P.G., 1974. The IP phase measurement and inductive coupling. Geophysics 39 (5), 650–665.
Heenan, J., Porter, A., Ntarlagiannis, D., Young, L.Y., Werkema, D.D., Slater, L.D., 2013. Sensitivity of the spectral induced polarization method to microbial enhanced oil recovery processes. Geophysics 78 (5), E261–E269.
Heenan, J., Slater, L.D., Ntarlagiannis, D., Atekwana, E.A., Fathepure, B.Z., Dalvi, S., Ross, C., Werkema, D.D., Atekwana, E.A., 2015. Electrical resistivity imaging for long-term autonomous monitoring of hydrocarbon degradation: lessons from the Deepwater Horizon oil spill. Geophysics 80 (1), B1–B11.
Hördt, A., Bairlein, K., Bielefeld, A., Bücker, M., Kuhn, E., Nordsiek, S., Stebner, H., 2016. The dependence of induced polarization on fluid salinity and pH, studied with an extended model of membrane polarization. Journal of Applied Geophysics 135, 408–417.
Kemna, A., 2000. Tomographic Inversion of Complex Resistivity - Theory and Application, Ph.D. Ruhr-University of Bochum.
Kemna, A., Binley, A., Slater, L., 2004. Crosshole IP imaging for engineering and environmental applications. Geophysics 69 (1), 97–107.
Kłonowski, M.R., Breedveld, G.D., Aagaard, P., 2008. Spatial and temporal changes of jet fuel contamination in an unconfined sandy aquifer. Water Air Soil Pollut. 188 (1–4), 9–30.
Lari, K.S., Rayner, J.L., Davis, G.B., 2018. Towards characterizing LNAPL remediation endpoints. J. Environ. Manag. 224, 97–105.
Löser, C., Seidel, H., Zehnsdorf, A., Stottmeister, U., 1998. Microbial degradation of hydrocarbons in soil during aerobic/anaerobic changes and under purely aerobic conditions. Appl. Microbiol. Biotechnol. 49 (5), 631–636.
Lu, J., Germain, R.S., Andrews, T., 2014. NAPL source identification utilizing data from laser induced fluorescence (LIF) screening tools. pp. 77–97.
Maurya, P.K., Balbarini, N., Møller, I., Rønde, V., Christiansen, A.V., Bjerg, P.L., Auken, E., Fiandaca, G., 2018. Subsurface imaging of water electrical conductivity, hydraulic permeability and lithology at contaminated sites by induced polarization (Geophysical Journal International). 213 (2), 770–785.
McCall, W., Christy, T.M., Pipp, D.A., Jaster, B., White, J., Goodrich, J., Fontana, J., Doxtader, S., 2018. Evaluation and application of the optical image profiler (OIP) a direct push probe for photo-logging UV-induced fluorescence of petroleum hydrocarbons. Environmental Earth Sciences 77 (10), 374.
Mewafy, F.M., Werkema Jr., D.D., Atekwana, E.A., Slater, L.D., Aal, G.A., Revil, A., Ntarlagiannis, D., 2013. Evidence that bio-metallic mineral precipitation enhances the complex conductivity response at a hydrocarbon contaminated site. J. Appl. Geophys. 98, 113–123.
Naudet, V., Gourry, J.C., Girard, F., Mathieu, F., Saada, A., 2014. 3D electrical resistivity tomography to locate DNAPL contamination around a housing estate. Near Surface Geophysics 12 (3), 351–360.
Olhoeft, G.R., 1985. Low-frequency electrical properties. Geophysics 50 (12), 2492–2503.
Osterman, G., Sugand, M., Keating, K., Binley, A., Slater, L., 2019. Effect of clay content and distribution on hydraulic and geophysical properties of synthetic sand-clay mixtures. Geophysics *84* (4), E239–E253.
Panagos, P., Van Liedekerke, M., Yigini, Y., Montanarella, L., 2013. Contaminated sites in Europe: review of the current situation based on data collected through a European network. Journal of Environmental and Public Health 2013.
Revil, A., Florsch, N., 2010. Determination of permeability from spectral induced polarization in granular media. Geophys. J. Int. 181 (3), 1480–1498.
Revil, A., Schmutz, M., Batzle, M.L., 2011. Influence of oil wettability upon spectral induced polarization of oil-bearing sands. Geophysics 76 (5), A31–A36.
Sauck, W.A., 2000. A model for the resistivity structure of LNAPL plumes and their environs in sandy sediments. J. Appl. Geophys. 44 (2–3), 151–165.
Schmutz, M., Revil, A., Vaudelet, P., Batzle, M., Viñao, P.F., Werkema, D.D., 2010. Influence of oil saturation upon spectral induced polarization of oil-bearing sands. Geophys. J. Int. 183 (1), 211–224.
Schwartz, N., Huisman, J.A., Furman, A., 2012. The effect of NAPL on the electrical properties of unsaturated porous media. Geophys. J. Int. 188 (3), 1007–1011.
Shefer, I., Schwartz, N., Furman, A., 2013. The effect of free-phase NAPL on the spectral induced polarization signature of variably saturated soil. Water Resour. Res. 49 (10), 6229–6237.
Slater, L., Lesmes, D.P., 2002. Electrical-hydraulic relationships observed for unconsolidated sediments. Water Resour. Res. 38 (10), 31.
Tang, J., Lu, X., Sun, Q., Zhu, W., 2012. Aging effect of petroleum hydrocarbons in soil under different attenuation conditions. Agric. Ecosyst. Environ. 149, 109–117.
Totsche, K.U., Kogel-Knabner, I., Haas, B., Scheibke, R., Geisen, S., 2003. Evidence for preferential flow and ageing of NAPL and NAPL borne contaminants in the unsaturated soil zone of a creosote contaminated site: a field study. J. Plant Nutr. Soil Sci. 166, 102–110.
Ustra, A., Slater, L., Ntarlagiannis, D., Elis, V., 2012. Spectral induced polarization (SIP) signatures of clayey soils containing toluene. Near Surface Geophysics 10 (6), 503–515.
Vanhala, H., 1997. Mapping Oil-contaminated Sand and Till with the Spectral Induced Polarization (SIP) Method. Geophysical Prospecting.
Werkema Jr., D.D., Atekwana, E.A., Endres, A.L., Sauck, W.A., Cassidy, D.P., 2003. Investigating the geoelectrical response of hydrocarbon contamination undergoing biodegradation. Geophys. Res. Lett. 30 (12).
Zimmermann, E., Huisman, J.A., Mester, A., van Waasen, S., 2019. Correction of phase errors due to leakage currents in wideband EIT field measurements on soil and sediments. Measurement Science and Technology 30 (8), 084002.